

## Buckling resistant graphene nanocomposites

M. A. Rafiee,<sup>1</sup> J. Rafiee,<sup>1</sup> Z.-Z. Yu,<sup>2</sup> and N. Koratkar<sup>1,a)</sup>

<sup>1</sup>Department of Mechanical, Aerospace and Nuclear Engineering, Rensselaer Polytechnic Institute, Troy, New York 12180, USA

<sup>2</sup>State Key Laboratory of Chemical Resource Engineering, College of Materials Science and Engineering, Beijing University of Chemical Technology, Beijing 100029, People's Republic of China

(Received 1 October 2009; accepted 7 November 2009; published online 2 December 2009)

An experimental study on buckling of graphene/epoxy nanocomposite beam structures is presented. Significant increase (up to 52%) in critical buckling load is observed with addition of only 0.1% weight fraction of graphene platelets into the epoxy matrix. Based on the classical Euler-buckling model, the buckling load is predicted to increase by  $\sim 32\%$ . The over 50% increase in buckling load observed in our testing suggests a significant enhancement in load transfer effectiveness between the matrix and the graphene platelets under compressive load. Such nanocomposites with high buckling stability show potential as lightweight and buckling-resistant structural elements in aeronautical and space applications. © 2009 American Institute of Physics. [doi:10.1063/1.3269637]

Graphene is a monolayer of  $sp^2$  bonded carbon atoms that can be viewed as an individual atomic plane extracted from graphite. Recent advances<sup>1,2</sup> in the production of bulk quantities of exfoliated graphene from graphite have enabled the synthesis of graphene polymer composites. Such composites show tremendous potential for mechanical properties enhancement due to their combination of high specific surface area, strong nanofiller-matrix adhesion and the outstanding mechanical properties of the  $sp^2$  carbon bonding network in graphene. While the majority of work on graphene based materials has focused on quantifying their tensile strength and Young's modulus,<sup>3,4</sup> the buckling stability of graphene composites has not yet been investigated. In this paper, we perform systematic compression tests to quantify the buckling behavior of graphene epoxy nanocomposites.

For a column under an axial compressive load, the smallest critical load which defines the onset of structural instability is given by Euler's equation<sup>5</sup>

$$P_{\text{Buckling}} = \pi^2 EI / L_e^2, \quad (1)$$

where  $P_{\text{Buckling}}$  is the critical buckling load,  $E$  is the elastic modulus of the column,  $L_e$  is the effective length of the column, and  $I$  is the moment of inertia of the cross section. The effective length  $L_e$  depends on the column boundary conditions. For fixed boundary conditions, the effective length is half of the gage length of the column. The specimens used in this study have a slenderness ratio  $L_e / \rho \approx 45$  (where  $\rho$  is the column radius), greater than the critical slenderness ratio  $SR_c \approx 40$ , which means that the column can be considered to be long and Euler's equation can be utilized. The slenderness ratio and the critical slenderness ratio are computed using<sup>6</sup>

$$\frac{L_e}{\rho} = \frac{L_{\text{gage}}/2}{\sqrt{I/A}}, \quad (2)$$

$$SR_c = \sqrt{\frac{E\pi^2}{\sigma_{pl}}}, \quad (3)$$

where  $L_{\text{gage}}$  is the gage length,  $I$  is the least moment of inertia of the cross section,  $A$  is the area of the cross section, and

$\sigma_{pl}$  is the proportional limit of the material. From the classical Euler equation, it is clear that addition of graphene reinforcement into the matrix material will increase the elastic modulus of the sample, causing a corresponding increase in the critical buckling load. Therefore, the buckling stability enhancement is expected to be proportional to the stiffening (i.e., the elastic modulus enhancement) of the composite structure.

The graphene platelets used in this study were synthesized [Fig. 1(a)] by the rapid thermal expansion of graphite oxide.<sup>1,2</sup> Graphite oxide was prepared by oxidizing natural graphite flakes with an average diameter of 48  $\mu\text{m}$  in a solution of sulfuric acid, nitric acid and potassium chlorate for 96 h. Thermal exfoliation of graphite oxide was achieved by placing the graphite oxide powder (200 mg) in a 200 mm inner diameter, 1 m long quartz tube that was sealed at one end. The other end of the quartz tube was closed using a rubber stopper. An argon inlet was then inserted through the rubber stopper. The sample was flushed with argon for 10 min, and the quartz tube was quickly inserted into a tube furnace preheated to 1050  $^\circ\text{C}$  and held in the furnace for  $\sim 30$  s. Rapid heating ( $>2000$   $^\circ\text{C}/\text{min}$ ) splits the bulk graphite oxide into graphene platelets (GPLs) due to the pressure generated by evolution of  $\text{CO}_2$  gas which helps to overcome the van der Waals forces.<sup>1,2</sup> Figure 1(b) shows a transmission electron microscopy (TEM) image of a typical GPL flake synthesized by the above approach and Fig. 1(c) shows a high resolution TEM (HRTEM) image indicating that the GPL flake is comprised of approximately three to four individual graphene sheets. The electron diffraction pattern [shown in the inset of Fig. 1(c)] confirms the signature of few-layered graphene.<sup>3</sup>

To fabricate the GPL/epoxy composites, the desired amount of GPL was first weighed and dispersed in acetone (ratio of 100 mL of acetone to 0.1 g of GPL) using an ultrasonic probe sonicator at high amplitude for 1.5 h in an ice bath. The epoxy (System 2000 Epoxy Resin, Fiberglast Inc., USA) was added to the mixture, and sonicated following the same procedure for another 1.5 h. Next, the acetone is evaporated off by heating the mixture on a magnetic stir plate using a Teflon coated magnetic bar for 3 h at 70  $^\circ\text{C}$ . Subsequently, the mixture is placed in a vacuum chamber for 12 h at 70  $^\circ\text{C}$  to ensure that all of the acetone has been removed.

<sup>a)</sup>Author to whom correspondence should be addressed. Electronic mail: koratn@rpi.edu.

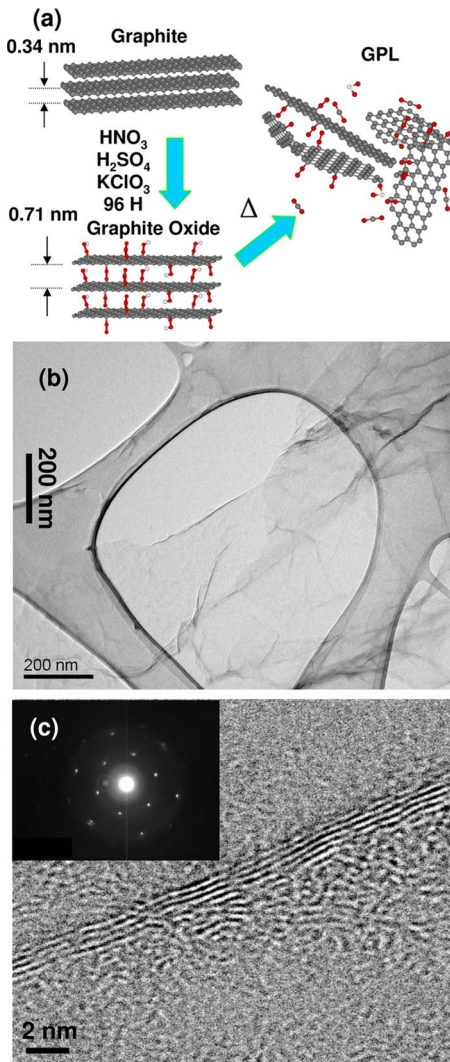


FIG. 1. (Color online) (a) Schematic illustration of the oxidation and thermal exfoliation process used to derive graphene platelets (GPL) from graphite. (b) TEM image of a typical GPL flake. (c) HRTEM of the GPL flake indicating that each flake is comprised of approximately three to four individual graphene sheets with the inset showing the measured electron diffraction pattern.

After allowing the GPL/epoxy slurry to cool down to room temperature to prevent any premature curing, a low viscosity curing agent (2120 Epoxy Hardener, Fiberglast Inc., USA) is added and subsequently mixed using a high speed shear mixer for 4 min at 2000 rpm. The mixture is again placed in a vacuum chamber to degas the epoxy for approximately 30 min. Finally, the mixture is poured into Silicon molds and the nanocomposite is cured at room temperature and 90 psi pressure for 24 h, followed by 4 h of postcure at 90 °C. The baseline epoxy and nanocomposite samples are ~90–100 mm in clamped length, ~24.5 mm in width, and ~3.5–3.9 mm in thickness. In addition to the GPL/epoxy composites we also prepared single-walled carbon nanotube (SWNT) and multiwalled carbon nanotube (MWNT) epoxy composites to compare the performance of carbon nanotube and graphene additives. The same protocols were used for SWNT and MWNT dispersion in the epoxy matrix. Note that in general carbon nanotubes are relatively easier to disperse than GPL, since the two-dimensional sheet geometry of GPL increases the probability of nanofiller entanglement and clustering. Therefore in order to ensure relatively uniform disper-

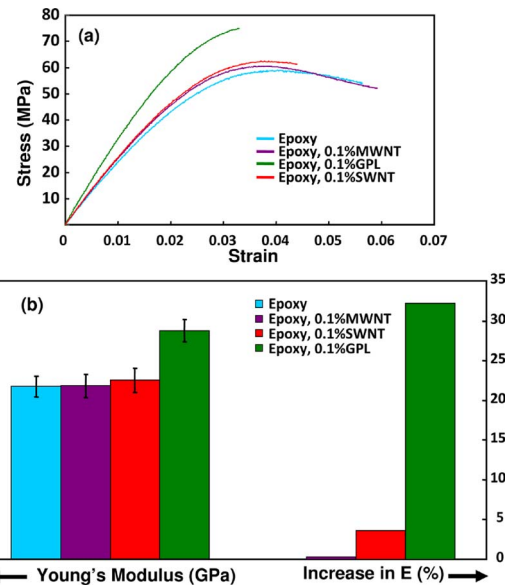


FIG. 2. (Color online) (a) Stress-strain response under tensile loading for the baseline epoxy and the nanocomposite samples. The modulus of the specimen is determined from the slope of the curves within the elastic limit. (b) Percentage increases in the elastic modulus of the baseline epoxy matrix and nanocomposite samples at a fixed nanofiller weight fraction of ~0.001 (i.e., 0.1%).

sion for all the three nanofiller systems (i.e., MWNT, SWNT, and GPL), we intentionally selected a low nanofiller weight fraction of ~0.001 (i.e., 0.1%) in our tests.

The tensile elastic modulus of the samples was measured prior to the buckling tests. An extensometer was attached to the specimen to measure the strain during the tests. The Young's moduli of the nanocomposites [Fig. 2(b)] were calculated from the slope of the stress-strain curves [Fig. 2(a)]. There was only ~0.5% increase in the Young's modulus of the 0.1 wt % MWNT nanocomposite compared to the neat epoxy, while the Young's modulus of the 0.1 wt % SWNT and 0.1 wt % GPL nanocomposites showed approximately ~4% and ~32% increase, respectively. Note that when computing the theoretical buckling load, the measured tensile modulus was used. We did not measure compressive modulus since the bowing of the specimen resulted in inaccurate strain measurement from the extensometer.

Having measured the elastic modulus of nanocomposites, the samples were then buckled by the application of a monotonically increasing compressive displacement to the specimen (at the rate of ~0.1 mm/min). The resulting typical load-displacement response [Fig. 3(a)] was used to determine the buckling load. At the point of buckling the system is unstable, with the displacement continuing to increase without any further increase of the load (i.e., the load response levels off). The measured buckling load from Fig. 3(a) has been scaled appropriately using

$$P_{\text{Buckling, Scaled}} = P_{\text{Buckling}} \frac{L^2 I_{\text{ref}}}{L_{\text{ref}}^2 I}, \quad (4)$$

where  $P_{\text{Buckling, Scaled}}$  is the scaled buckling load used for comparison,  $P_{\text{Buckling}}$  is the buckling load obtained from the experiment,  $L$  is the clamped length of the nanocomposite,  $I$  is the moment of inertia of the nanocomposite,  $L_{\text{ref}}$  is the clamped length of the reference (pure epoxy), and  $I_{\text{ref}}$  is the moment of inertia of the reference (pure epoxy) samples. The scaling of the buckling load [Eq. (4)] with the epoxy beam

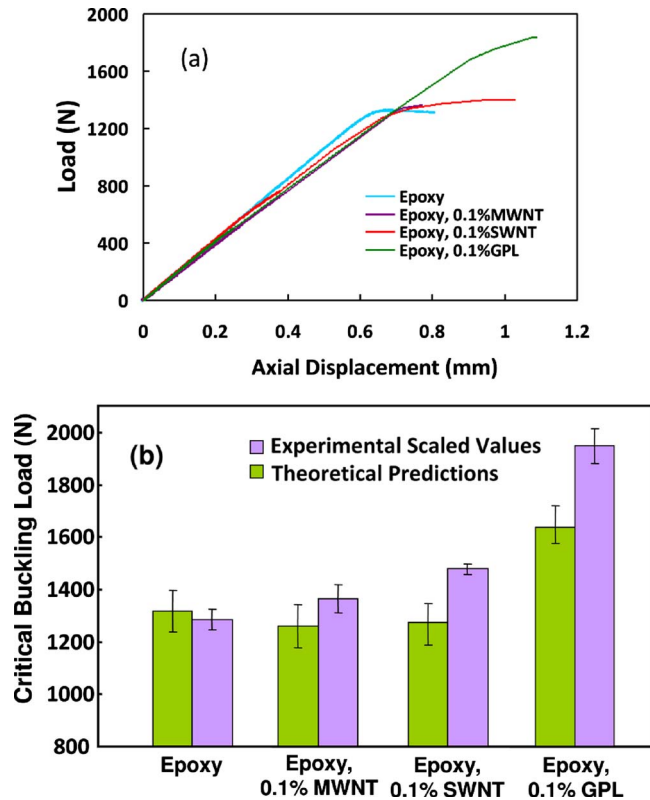


FIG. 3. (Color online) (a) Load-displacement response in compression used to determine the critical buckling load. (b) Predicted Euler's critical buckling load based on the increase in elastic modulus vs the actual buckling load measured in the experiment. The under-prediction of Euler's column buckling formula indicates a significant enhancement in load-transfer effectiveness between the polymer and the additives when subjected to a compressive load.

dimensions taken as a reference allows us to directly compare the buckling loads of the specimens. This is necessary to account for slight variations in the clamped length, thickness, and width of the samples. For the baseline epoxy specimen, the average scaled buckling load [Fig. 3(b)] is  $\sim 1285$  N, which is in reasonable agreement with the theoretical prediction ( $\sim 1316$  N) based on classical Euler buckling [Eq. (1)] and the measured tensile modulus [Fig. 2(b)]. Figure 3(b) indicates that with the addition of 0.1 wt % MWNT to the epoxy matrix, the average scaled buckling load is increased by  $\sim 6.2\%$  to 1363 N. For 0.1 wt % of SWNT the critical buckling load increases to 1477 N (a 15% increase). At the same nanofiller loading fraction of 0.1%, the GPL far out-performs the SWNT and MWNT additives and shows  $\sim 52\%$  increase in the critical buckling load to 1947 N.

According to the classical Euler buckling equation, the buckling load is a function of geometry and elastic modulus of the material. Since the critical buckling load is corrected for geometry variation by proper scaling [Eq. (4)], the increase in the buckling load should be accounted for by the increase in the elastic modulus of the nanocomposites compared to the pristine epoxy. Therefore, we expect the buckling loads to increase by 0.5%, 4%, and 32% [based on the increase in the elastic modulus, Fig. 2(b)] upon the addition of MWNT, SWNT, and GPL, respectively. Nonetheless, the test data indicates 6% (for MWNT), 15% (for SWNT), and 52% (for GPL) increases in the critical buckling load. This

suggests that the elastic modulus of the carbon nanotube and graphene composites under large compressive loading (more specifically, at the onset of buckling) is significantly enhanced compared to tensile loading. Enhanced load transfer in carbon nanotube composites under compressive load has been reported by Schadler *et al.*<sup>7</sup> When the specimen is subjected to a tensile load, possibly only the peripheral surface of the nanotube bundles that are bonded to the epoxy matrix are effective for load transfer, and the weak intertube bonding<sup>8–10</sup> contributes little to the load transfer. In contrast, when the specimen is subjected to compression, high compressive stress might force the polymer to infiltrate the nanotube bundles, creating a larger interaction zone<sup>8</sup> between the polymer and the nanotube bundles, and thus improving the polymer-nanotube load transfer.

What is interesting is that similar to nanotubes an enhancement in the load transfer effectiveness under compressive stress is also observed for graphene platelets. HRTEM characterization [Fig. 1(c)] indicates that in our system the graphene platelets are comprised of approximately three to four individual graphene sheets. Similar to nanotube bundles, only the outer graphene sheets are expected to contribute to load transfer under tension, while under compression the load may be shared more equitably by the sheets. Another consideration is that individual graphene sheets within clusters are expected to buckle and bend under compressive stress due to their atomic scale thickness. This bowing (or bending) of individual graphene sheets within clusters can increase frictional interlocking between the sheets and thus provide better sheet-to-sheet load transfer within the platelet. To summarize, graphene nanocomposites show potential to provide significant enhancement in buckling stability, which is an important consideration for the design of ultra lightweight and highly optimized structural elements used in aerospace applications.

N.K. acknowledges funding support from the U.S. Office of Naval Research (Award No. N000140910928) and the U.S. National Science Foundation (Award No. 0900188).

- <sup>1</sup>H. C. Schniepp, J.-L. Li, M. J. McAllister, H. Sai, M. Herrera-Alonso, D. H. Adamson, R. K. Prud'homme, R. Car, D. Saville, and I. A. Aksay, *J. Phys. Chem. B* **110**, 8535 (2006).
- <sup>2</sup>M. J. McAllister, J.-L. Li, D. H. Adamson, H. C. Schniepp, A. A. Abdala, J. Liu, M. Herrera-Alonso, D. L. Milius, R. Car, R. K. Prud'homme, and I. A. Aksay, *Chem. Mater.* **19**, 4396 (2007).
- <sup>3</sup>S. Stankovich, D. A. Dikin, D. Dommett, K. Kohlhaas, E. J. Zimney, E. A. Stach, R. D. Piner, S. T. Nguyen, and R. S. Ruoff, *Nature (London)* **442**, 282 (2006).
- <sup>4</sup>T. Ramanathan, A. A. Abdala, S. Stankovich, D. A. Dikin, M. Herrera-Alonso, R. D. Piner, D. H. Adamson, H. C. Schniepp, X. Chen, R. S. Ruoff, S. T. Nguyen, I. A. Aksay, R. K. Prud'homme, and L. C. Brinson, *Nat. Nanotechnol.* **3**, 327 (2008).
- <sup>5</sup>J. Singer, J. Arbocz, and T. Weller, *Buckling Experiments: Experimental Methods in Buckling of Thin-Walled Structures* (Wiley, New York, 1998), Vol. 1.
- <sup>6</sup>F.-H. Cheng, *Applied Strength of Materials* (Macmillan, New York, 1986).
- <sup>7</sup>L. S. Schadler, S. C. Giannaris, and P. M. Ajayan, *Appl. Phys. Lett.* **73**, 3842 (1998).
- <sup>8</sup>W. Zhang, J. Suhr, and N. Koratkar, *Adv. Mater.* **18**, 452 (2006).
- <sup>9</sup>J. Suhr, N. Koratkar, P. Keblinski, and P. Ajayan, *Nature Mater.* **4**, 134 (2005).
- <sup>10</sup>W. Zhang, I. Srivastava, Y.-F. Zhu, C. R. Picu, and N. Koratkar, *Small* **5**, 1403 (2009).